JMEPEG (2009) 18:88–94
DOI: 10.1007/s11665-008-9264-y

1059-9495/$19.00

Corrosion Protection of In Situ Al-Based Composite by Cerium Conversion Treatment

S.C. Tjong and H.W. Huo

(Submitted November 8, 2007; in revised form May 13, 2008)

Cerium conversion films were deposited on the surface of in situ aluminum-based composite in solutions containing different cerium chloride ($CeCl_3$) and hydrogen peroxide (H_2O_2) concentrations at 30 °C. The morphology and composition of conversion films deposited in various solutions were investigated using scanning electron microscopy, energy dispersive x-ray analysis, and x-ray photoelectron spectroscopy (XPS). SEM observations revealed that only patches of film can be deposited on the composite surface when immersed in solutions with low $CeCl_3$ and H_2O_2 concentrations. However, entire composite surface was covered with a compact film when immersed in a solution containing 10 g/L $CeCl_3$ and 100 mL/L H_2O_2. XPS results indicated that cerium was incorporated as Ce^{4+} species in the hydrated oxide film. The formation of such hydrated conversion film on the composite resulted in low anodic current density and more noble pitting potential when exposed to 3.5% NaCl solution.

Keywords chloride, coatings, composites, corrosion, oxide film

1. Introduction

Due to increasing demand on lightweight materials in industrial sectors, aluminum-based metal matrix composites (MMCs) have become increasingly used for critical structural applications because of their excellent stiffness to density and strength to density ratios. Discontinuous short fibers, whiskers, and particulates are typical fillers commonly used to reinforce the Al-based MMCs. Particle-reinforced MMCs possess distinct advantages over fiber reinforced composites in terms of their low cost and isotropic mechanical properties considerations. The ex situ MMCs can be prepared by introducing ceramic particulates into aluminum or its alloys via ingot casting and powder metallurgy (PM) processes. However, agglomeration of ceramic particulates often occurs during the fabrication of ex situ MMCs. Moreover, the sizes of ex situ ceramic particulates are very large, typically in the range of tens to hundreds of micrometers. Such large ceramic particulates fracture readily during mechanical loading, leading to the composites exhibit poor mechanical performances. In this respect, novel processing techniques based on the in situ production of reinforced ceramic particles have been developed. These techniques include exothermic dispersion (XD), reactive hot pressing (RHP), combustion-assisted cast and direct reaction synthesis (Ref 1-3). Among these, RHP process is attractive due to their simplicity and flexibility. In the process, ultrafine ceramic particulates are formed in situ by the exothermic reaction between the element constituents of composites under hot pressing conditions. The reduction in the particle size is beneficial to improve the mechanical strength of the MMCs.

Silicon carbide particles are frequently used to reinforce the Al-based alloys due to their low cost and availability. However, SiC particles react readily with aluminum during processing, yielding Al_4C_3 interfacial product. This results in the composites having poor mechanical properties. Titanium diboride (TiB_2) has distinct advantages over SiC because of its inertness to aluminum. In other words, formation of brittle reaction products at the reinforcement-matrix interface can be avoided using the TiB_2 particles. Moreover, TiB_2 particles exhibit high-elastic modulus and hardness, high melting point, and electrical conductivity as well as good thermal stability (Ref 4). Accordingly, several studies have been conducted in recent years to synthesize the in situ TiB_2 particulate reinforced Al-based composites with enhanced mechanical properties (Ref 5-8).

The ex situ Al-based MMCs have been used as impellers and agitators in marine environments. However, pitting corrosion is the major problem that leads to severe degradation of ex situ MMCs in marine environments. To facilitate the application of in situ Al-based MMCs in chloride-containing environments, their pitting corrosion behavior and protection must be properly understood. In a previous study, we have investigated the corrosion behavior of Al-based composites containing in situ TiB_2, Al_2O_3, and Al_3Ti reinforcements in aerated 3.5% NaCl solution (Ref 9). The results showed that these composites were also susceptible to the pitting corrosion when exposed to a chloride environment.

Chromate conversion coatings have been used extensively to protect the aluminum from pitting corrosion. Due to the toxicity of chromate, the use of environmentally friendly rare-earth metal conversion coatings for corrosion protection of aluminum alloys has attracted increasing attention of materials scientists. It is generally known that the additions of rare-earth metal ions such as Ce^{3+}, Y^{3+}, La^{3+}, Pr^{3+}, Nd^{3+} to the chloride

S.C. Tjong, Department of Physics and Materials Science, City University of Hong Kong, Tat Chee Avenue, Kowloon, Hong Kong; and **H.W. Huo**, College of Life and Chemical Sciences, Shenyang Normal University, Shenyang 110034, P.R. China. Contact e-mail: aptjong@cityu.edu.hk.

containing solutions can improve the pitting corrosion resistance of metallic alloys (Ref 10-13). Corrosion inhibition by cerium salts is associated with the formation of insoluble hydrated cerium oxide film over cathodic sites on the alloy surface. Thus the insoluble hydroxides act as effective cathodic inhibitors by suppressing kinetics of the oxygen reduction at cathodic sites of aluminum alloy surfaces (Ref 11). To accelerate the formation of a cerium oxide/hydroxide film, further addition of hydrogen peroxide or sodium perchlorate to the cerium chloride bath is needed (Ref 14). Similarly, rare-earth conversion coatings are also reported to be beneficial in improving the pitting corrosion resistance of ex situ Al-based composites (Ref 15-19). Chen and Mansfeld modified the surface of an Al 6092/SiC_p composite through anodizing in sulfuric acid followed by sealing in either hot water or cerium nitrate solutions (Ref 15). They reported that sealing in cerium nitrate provided better corrosion protection for the composite. Hamdy et al. indicated that the degree of corrosion protection of Al-based composite depends on the specimen preparation or surface modification prior to cerium pretreatment (Ref 16). Pitting corrosion occurs in the composite specimen immersed directly in cerium chloride solution due to the formation of very thin film of cerium oxide. Anodizing in boiling distilled water is necessary for corrosion protection prior to cerium salt treatment. This is because cerium can be incorporated into the pores of thick anodized film to block the active surface sites. More recently, Pardo et al. studied the effects of lanthanum and cerium-based treatments on the corrosion behavior of A360/SiC_p and A380/SiC_p composites (Ref 17, 18). The composites without treatment are susceptible to localized corrosion as a result of their heterogeneous microstructure. The pits nucleated preferentially at the matrix-SiC_p and matrix/intermetallic compounds interfaces, leading to high corrosion rates. Both Ce and La treatments reduce the corrosion rate and localized pitting attack. The protection mechanism is associated with the formation of CeO_2 or La_2O_3 over intermetallic compounds, SiC_p and Si eutectic, thereby blocking the cathodic reaction of the corrosion process. There is no information available in the literature relating the corrosion protection of in situ Al-based composites with rare-earth conversion film. It is considered that the rare-earth conversion films can offer a high degree of protection for the in situ Al-based composites immersed in marine environments. This work aims to study the effect of cerium oxide conversion film on the Al-based composite reinforced with Al_2O_3 and TiB_2 in situ particles. The conversion film formed on the in situ Al-based composite was characterized using scanning electron microscopy (SEM), energy dispersive x-ray analysis (EDX), and x-ray photoelectron spectroscopy (XPS).

2. Experimental Procedure

2.1 Cerium Conversion Treatment

The Al-based composite reinforced with in situ Al_2O_3 and TiB_2 submicron particulates was prepared from the Al-TiO_2-B system with B/TiO_2 ratio of 6/3 via RHP process. The preparation of such in situ Al-based composite had been reported previously (Ref 20-22). Herein we briefly described its synthesis via RHP from the Al-TiO_2-B system. In the process, the powders were ball milled in alcohol for 8 h and then dried. The cold compacted powder mixture was heated to above 800 °C in a vacuum and maintained for 10 min, then cooled down to 600 °C and hot pressed at ~150 MPa. The pressed billets were extruded at an extrusion ratio of 20:1 at 420 °C.

The chemical reactions between the Al, TiO_2, and B powders during RHP take place as follows:

$$3TiO_2 + 13Al \rightarrow 2Al_2O_3 + 3Al_3Ti \quad \text{(Eq 1)}$$

$$3TiO_2 + 6B + 4Al \rightarrow 2Al_2O_3 + 3TiB_2 \quad \text{(Eq 2)}$$

When boron is absent, only TiO_2 reacts with Al, leading to the formation of Al_2O_3 and brittle Al_3Ti phases (reaction 1). The amount of Al_3Ti phase can be reduced by adding B to the TiO_2-Al system. Further, B addition also induces the formation of TiB_2 particles (reaction 2). The amounts of Al_2O_3, TiB_2, and Al_3Ti phases can be controlled by varying the boron content. When the B/TiO_2 molecular weight ratio reaches 6/3, the Al_3Ti phase can be eliminated. Under this condition, only Al_2O_3 and TiB_2 particles are in situ formed within aluminum matrix. The actual volume contents of in situ Al_2O_3 and TiB_2 reinforcing particles determined from the x-ray diffraction technique were 11.7% and 8.7%, respectively. The microstructure of the composite is shown in Fig. 1. The in situ TiB_2 particles exhibit hexagonal appearances and distribute uniformly within aluminum matrix of the composite.

Cylinder specimens for conversion treatment were cut from the composite. Prior to the conversion treatment, the specimens were ground down to 1200 grit silicon carbide paper and degreased. They were then immersed in solutions containing different $CeCl_3$ and H_2O_2 concentrations under pH 2.5 at 30 °C for 1 h (Table 1). After conversion treatment, the specimens were rinsed with distilled water and dried.

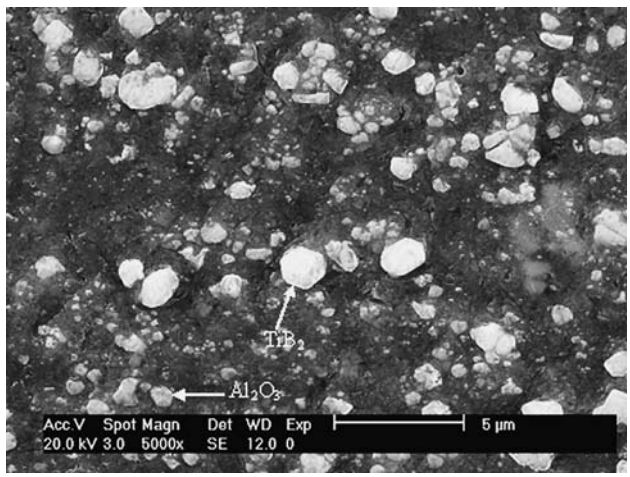

Fig. 1 Typical microstructure of Al-based composite reinforced with in situ Al_2O_3 and TiB_2 particulates. The TiB_2 particulates exhibit hexagonal morphology

Table 1 Composition of conversion solutions at pH of 2.5

Solution	1	2	3	4
$CeCl_3 \cdot 7H_2O$, g/L	3.0	6.0	10.0	15.0
H_2O_2, mL/L	20	50	100	200

2.2 Characterization of Conversion Films

The conversion films were characterized using SEM, EDX and XPS. Prior to SEM observation, the specimens were coated with Au film to reduce undesirable charging effects. The XPS measurements were carried out using a Physical Electronics Industries (PHI 5802 system) equipped with a standard Al $K\alpha$ x-ray source (1486.6 eV) and a hemispherical analyzer. The pressure in the specimen chamber was kept at about 1×10^{-9} Torr.

2.3 Electrochemical Measurements

The electrochemical measurements were carried out using a Princeton Applied Research (PAR) potentiostat (Model 273A) equipped with M 352 corrosion measurement software. A three-electrode electrochemical cell consisted of working electrode, saturated calomel electrode (SCE), and graphite counter electrode was used. The variations of the open circuit potential (E_{ocp}) with time of the composite specimens during conversion treatment in solutions containing different $CeCl_3$ and H_2O_2 concentrations were recorded.

The potentiodynamic polarization tests of untreated and cerium chloride treated specimens in aerated 3.5 wt.% NaCl solution at 25 °C were also performed. Paint suitable for marine environment was used to mask the specimen-epoxy boundary to avoid the crevice corrosion. After stabilization of E_{ocp}, the potentiodynamic scan was initiated from −150 mV with respect to the E_{ocp} toward anodic direction at a rate of 0.5 mV s^{-1}. The measurements were repeated twice to ensure reproducibility of the test results.

For cyclic voltammetry test, the solutions used were 10 g/L $CeCl_3$, and 10 g/L $CeCl_3$ with 100 mL/L H_2O_2. The measurement was started from the open circuit potential and scanned toward cathodic direction. The scan direction was reversed when the potential reached a value of −1.0 V with respect to open circuit potential. It was then terminated at the open circuit potential. The scan rate employed was 50 mV s^{-1}.

3. Results and Discussion

3.1 Potential-Time Characteristics

Figure 2 shows the variations of the open circuit potential with time for the composite specimens immersed in solutions containing different $CeCl_3$ and H_2O_2 contents with pH of 2.5 at 30 °C for 1 h. The compositions of the solutions are listed in Table 1. During the measurements, the potentiostat monitors and records the electrode potential of the specimens immersed in solutions investigated for every 50 s. Such signal is then sent to a personal computer and stored. When the electrode is immersed in the solution, the negative shift of the potential implies the dissolution of the original oxide film formed on the specimen, i.e., surface activation. In contrast, the positive shift of the potential indicates the formation of a protective film and an increase in the passive film thickness. For solutions 1 and 2, the open circuit potential of the composite shifts toward more negative direction with increasing immersion time. Thus no protective film is formed on the specimen. For solution 3, the potential of the specimen shifts toward negative direction during the first 860 s immersion, and then reversely displaces toward anodic direction. After ~2000 s, the potential stabilizes

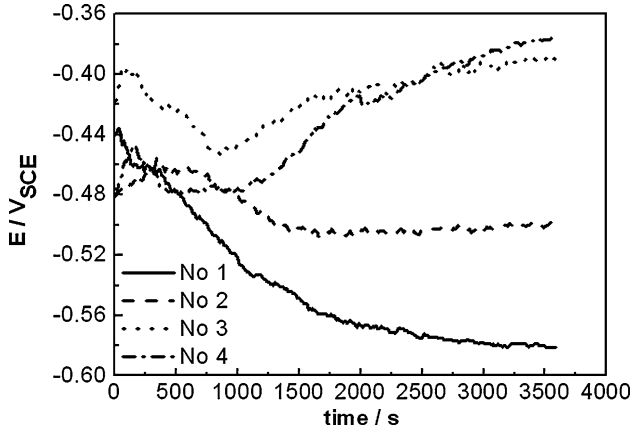

Fig. 2 Open circuit potential vs. time curves for the composite specimens immersed in solutions containing different $CeCl_3$ and H_2O_2 contents for 1 h

at −0.39 V_{SCE}. At this stage, a protective film is formed on the composite after initial surface activation during conversion treatment. For solution 4, the variation trend of the potential with time is similar to that of solution 3. For these four solutions having the same pH, it is evident that the open circuit potential of the specimen depends greatly on the Ce^{3+} and H_2O_2 concentrations of the solutions. When the in situ composite is immersed in $CeCl_3$ solution containing H_2O_2, the potential difference between the reinforced particles and the aluminum matrix favors formation of local micro cells. The main electrochemical reactions take place during immersion can be described as follows:

$$Al \rightarrow Al^{3+} + 3e \quad \text{(Eq 3)}$$

$$O_2 + 2H_2O + 4e \rightarrow 4OH^- \quad \text{(Eq 4)}$$

In the process, TiB_2 and Al_2O_3 reinforcing particles of the composite investigated are considered to act as the cathodes, thus the pH near these particles increases due to the cathodic reaction. When a critical pH for forming cerium conversion film is reached, the film would precipitate on the cathode sites initially. The oxidizing agent, H_2O_2, of the conversion solution is decomposed into water and oxygen according to the following reaction:

$$2H_2O_2 \rightarrow 2H_2O + O_2 \quad \text{(Eq 5)}$$

The O_2 released from H_2O_2 then takes part in the reduction reaction at the cathodic sites. The H_2O_2 oxidizing agent accelerates formation of the conversion film to a very short period of time, i.e., 1 h. From Table 1, the H_2O_2 concentration of solution 1 is quite low, thus only limited O_2 is released into the solution. This leads to a lack of O_2 at the cathodic sites for oxygen reduction reaction to take place. Under this condition, formation of the cerium conversion film is rather difficult. For solution 2 containing higher Ce^{3+} and H_2O_2 contents, the open circuit potential displaces to a more positive value compared to that of the solution 1. With further increasing the concentrations of H_2O_2 and Ce^{3+} in solution 3, the oxygen reduction reaction occurs more readily on the specimen surface. Consequently, the pH of the local cathodic sites increases and this facilitates the deposition of cerium conversion film from the solution.

Apparently, hydrogen peroxide is critical to formation of oxide film on the electrode surface. Figure 3 shows the cyclic voltammetric curves of the composite specimen immersed in 10 g/L $CeCl_3$ solution, and 10 g/L $CeCl_3$ solution containing 100 mL/L H_2O_2. It can be seen that the addition of H_2O_2 obviously affects the cathodic reaction on the surface of electrode. The characteristic potential of H_2O_2 decomposition was found to be about −0.65V.

3.2 Morphology of the Conversion Film

Figure 4(a-d) shows the surface morphologies of cerium conversion films formed on the composite specimens immersed in different solutions. From Fig. 4(a) and (b), Ce-rich film just covers some local areas of the specimen surface. This is as expected because the Ce^{3+} and OH^- concentrations of the solutions 1 and 2 are quite low. However, entire surface of the specimen immersed in solution 3 is covered by a conversion film with "dry mud" morphology (Fig. 4c). This implies that the solution 3 favors formation of a compact conversion film. Severe cracks can be observed in the conversion film with further increasing the Ce^{3+} and H_2O_2 concentrations in solution 4. This is because Ce-rich agglomerates are precipitated on the conversion film due to an increase of the precipitation rate (Fig. 2c). The EDX results for selected areas as marked as A, B, C, and D in Fig. 4(a-d) are listed in Table 2. Apparently, the conversion films consist mainly of cerium and aluminum. Titanium is originated from a pear-liked region with a depth of a few micrometers below the composite surface during the EDX measurement. We consider that the conversion films do not contain titanium. Electron spectroscopic method such as XPS is an effective tool to determine the surface composition and valency states of the elements in the conversion film.

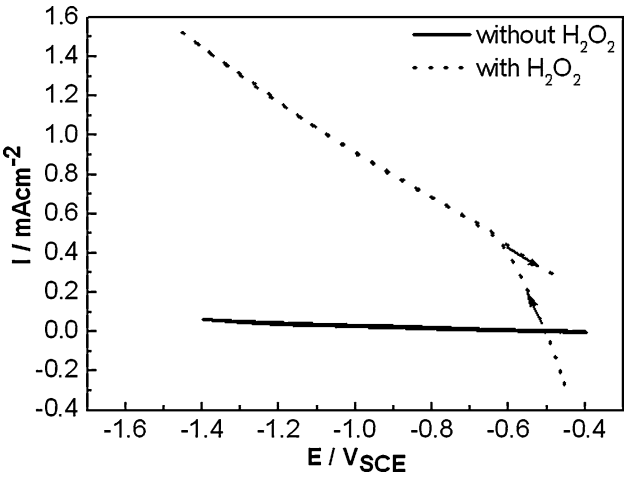

Fig. 3 Cyclic voltammetric curves of the composite specimen immersed in 10 g/L $CeCl_3$ solution, and 10 g/L $CeCl_3$ solution containing 100 mL/L H_2O_2

Table 2 Composition (at. %) for the selected areas in the conversion films as shown in Fig. 4a-d determined by EDX

Area	O	Al	Ti	Ce	Au
A	61.33	31.31	2.78	3.3	1.28
B	61.47	30.25	2.83	4.2	1.25
C	53.38	31.49	3.26	5.89	5.98
D	55.99	26.18	2.62	7.98	7.33

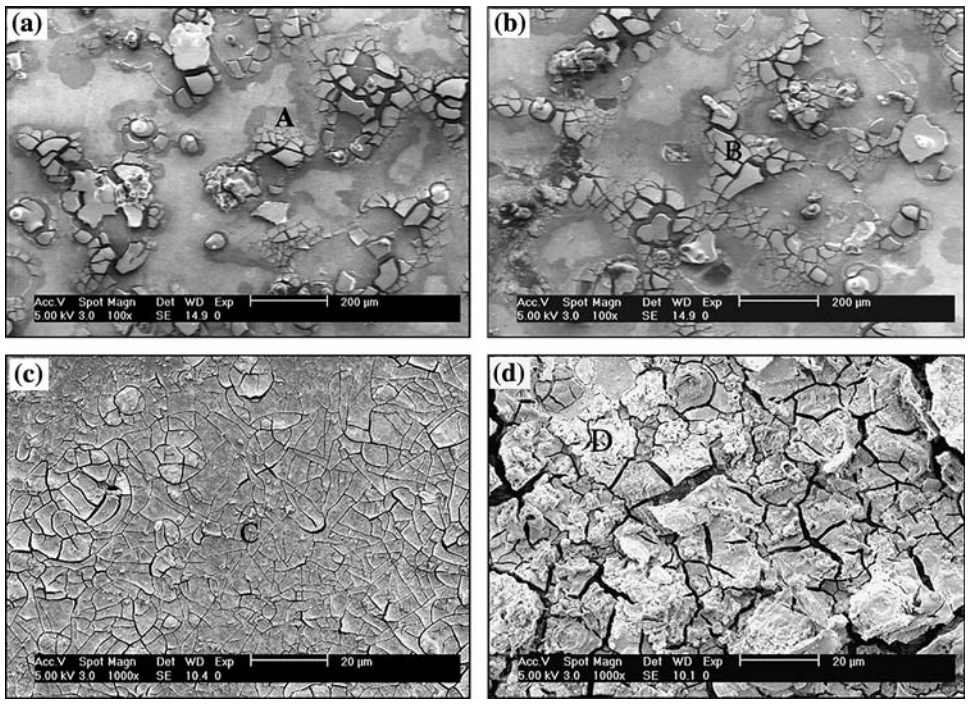

Fig. 4 Surface morphologies of the cerium conversion films formed on the composite specimens immersed in (a) solution 1, (b) solution 2, (c) solution 3, and (d) solution (4)

3.3 Composition of the Conversion Film

Figure 5 shows the XPS survey scan spectrum of the conversion film immersed in solution 3. It is evident that Ce, O, C, and Al elements are present in the conversion film. The carbon comes from contaminated hydrocarbon species on the specimen. Thus, the conversion film consists of mixed cerium/aluminum oxides and hydroxides. The hydrocarbon species originate from the solutions and specimens. It also can be deposited from air to the composite surfaces during insertion of the specimens into XPS spectrometer. The specimens were washed with distilled water prior to XPS measurement. However, XPS spectrometer is surface sensitive and can detect extremely small amount of hydrocarbon species (e.g., C_2H_2) on the specimen surfaces. Figure 6 shows the XPS Ce3d spectrum of the conversion film. According to the literature, the Ce3d spectrum of CeO_2 exhibits characteristic $3d_{5/2}$ peak at 881.6 eV, $3d_{3/2}$ peak at 899.9 eV and satellite peak at 916 eV (Ref 23-25). The interpretation of satellite peak is rather complicated. It could arise from electronic transitions such as shake-down or shake-up (Ref 26), or from electron interactions such as multiplet splitting or hybridization (Ref 27) during photoemission process. Shake-up like occurs when an outer shell electron is excited to an unoccupied orbital during photoemission. This leads to an energy loss as a result of electron excitation. Multiplet splitting is resulted from an interaction between spin of excited electrons with valence unpaired electrons. Hybridization is associated with an interaction between cerium and its neighboring atoms. Despite the disagreement in interpretation of satellite peak of the Ce3d spectrum, the satellite peak is generally used as an indicator for the presence Ce^{4+} species as such a peak is missing in the 3d spectrum of Ce^{3+} species. From Fig. 6, the Ce3d spectrum of conversion film also shows a distinct satellite peak at 915.9 eV, demonstrating that the film consists mainly of Ce^{4+} instead of Ce^{3+}. It is considered that the H_2O_2 oxidizing agent promotes oxidation of Ce^{3+} from solution 3 with into Ce^{4+} species during the film deposition. The addition of H_2O_2 facilitates deposition of $Ce(OH)_4$ or $CeO_2 \cdot H_2O$ from a cerium salt solution via the following reactions (Ref 28):

$$2Ce^{3+} + H_2O_2 + 2OH^- \rightarrow 2Ce(OH)_2^{2+} \quad \text{(Eq 6)}$$

$$Ce(OH)_2^{2+} + 2OH^- \rightarrow CeO_2 \cdot 2H_2O \quad \text{(Eq 7)}$$

The formation of cerium hydroxide or hydrated cerium oxide can be verified from the O1s spectrum of conversion film. Figure 7 shows the O1s spectrum of the conversion film. The O1s spectrum of the conversion film prior to sputtering is relatively broad with a full width at half maximum (FWHM) of more than 4 eV. Thus, this spectrum can be deconvoluted at least into two peaks located at 529.6 and 531.5 eV, respectively. A Gaussian peak profile was used to fit the O1s spectrum. The binding energy located at 529.6 eV is assigned as O^{2-} bonding (M-O) associated with the Ce^{4+} and Al^{3+} species. The binding energy located at 531.5 eV is assigned as OH^- bonding (M-OH) associated with hydrated Ce^{4+} species. The peak height and area of the M-OH deconvoluted peak are comparable to those of M-O peak. The presence of a large amount of M-OH content in conversion film enhances its corrosion

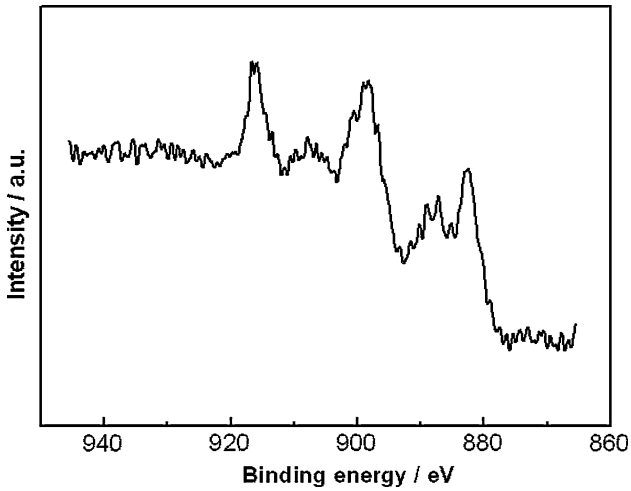

Fig. 6 XPS Ce3d spectrum of the conversion film prepared from solution 3

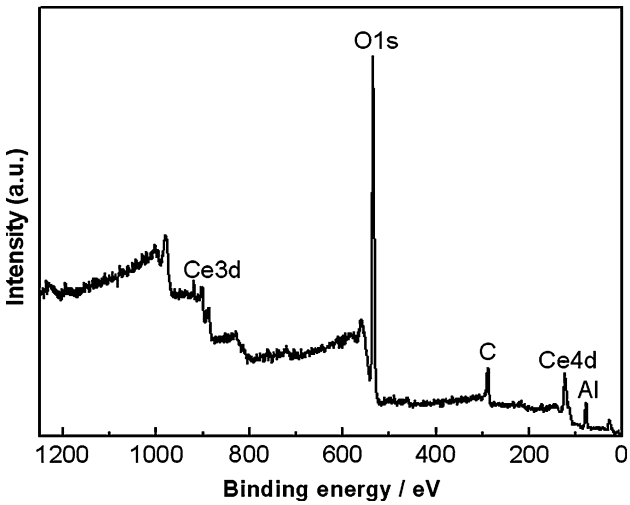

Fig. 5 XPS survey scan spectrum of the conversion film formed on the composite specimen immersed in solution 3

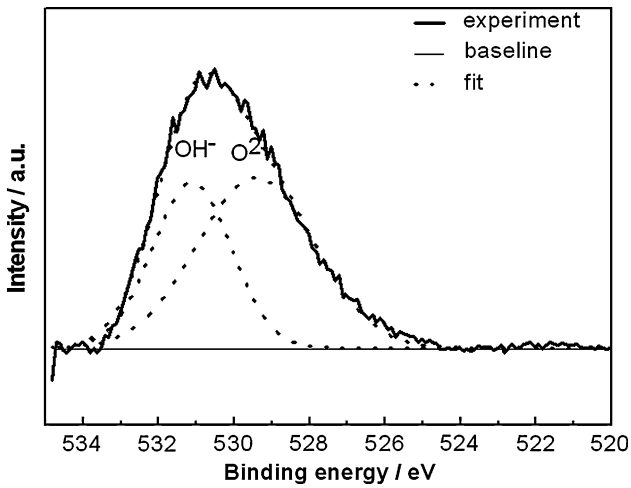

Fig. 7 Deconvolution O1s spectrum for the conversion film prepared from solution 3

resistance considerably (Ref 29). Consequently, the conversion film exhibits self-healing behavior on exposure to chloride environments (Ref 30). In this regard, cerium conversion film is expected to exhibit large passivation range when exposed to chloride containing solutions.

3.4 Potentiodynamic Polarization Behavior

Figure 8 shows the potentiodynamic polarization curves of the composite specimens coated with conversion films exposed in 3.5 wt.% NaCl solution. The polarization curve of pristine composite is also shown for the purpose of comparison. The corrosion current density of the bare composite is $\sim 5.82 \times 10^{-6}$ A cm^{-2}. The conversion treatment is very effective to reduce the corrosion current density of the composite. The improvement of the corrosion resistance of the composite specimens depends greatly on the $CeCl_3$ and H_2O_2 concentrations. For solution 1, the degree of protection is limited due to the formation of conversion film on localized areas of the composite surface as mentioned above. By increasing the covering and uniformity of conversion film, the corrosion current density decreases substantially. The corrosion current density decreases to 2.16×10^{-8} A cm^{-2} for the composite treated in solution 3. Furthermore, the anodic passivation range for the conversion-coated composite specimens is much larger than that of untreated composite. The pitting potential (E_{pit}) of treated composite specimens is more noble than that of untreated counterpart. The E_{pit} values for the untreated and solution 3 treated composite specimens are determined to be −681 and −188 mV, respectively. For the specimen treated in solution 4, the corrosion current density and E_{pit} are 1.8×10^{-7} A cm^{-2} and −371 mV, respectively. The corrosion resistance is reduced when compared to the composite treated in solution 3. This is due to the formation of severe cracks in the conversion film. The higher corrosion resistance of the conversion film is associated with the formation of a uniform cerium oxide/hydroxide film covering the whole surface. Bethencourt et al. reported that the corrosion protection afforded by the cerium-containing films derives from the suppression of the cathodic oxygen reduction reaction (Ref 30). It is believed that the cerium oxide/hydroxide film creates a barrier to either the supply of oxygen to, or the supply of electrons from, the metal. Both of these processes are necessary for the oxygen reduction reaction at cathodic sites. The suppression of the cathodic half of the corrosion reaction retards the overall corrosion rate.

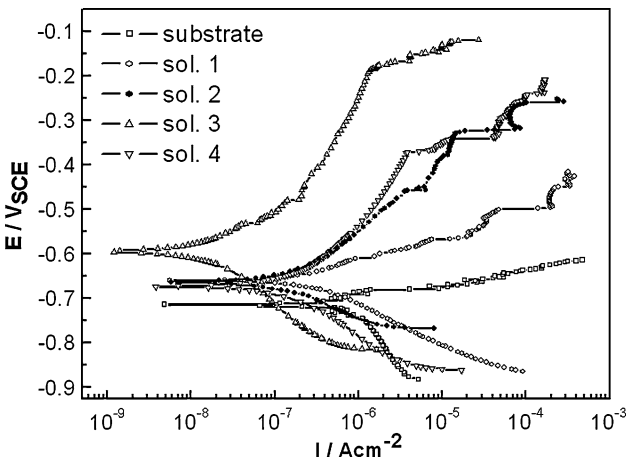

Fig. 8 Potentiodynamic polarization curves of untreated and cerium chloride treated composite specimens in 3.5 wt.% NaCl solution

4. Conclusions

Series of solutions containing different concentrations of cerium chloride and hydrogen peroxide (H_2O_2) at 30 °C were used to form protective conversion films on in situ Al-based composite. A compact film covering entire surface of the specimen can be deposited on the composite when immersed in 10 g/L and 100 mL/L $CeCl_3$ and H_2O_2 at 30 °C as demonstrated by the potential-time measurements and SEM observations. XPS results indicated that cerium was incorporated as Ce^{4+} species in the hydrated oxide film. The compact conversion film improved the corrosion resistance exposed to NaCl solution. These were featured by reduction in corrosion current and anodic current densities, displacement of corrosion potential and pitting potential to more positive values.

References

1. T. Nukami and M.C. Flemings, In Situ Synthesis of TiC Particulate-Reinforced Aluminum Matrix Composites, *Metall. Mater. Trans. A*, 1995, **26**, p 1877–1884
2. P. Li, E.G. Kandalova, and V.I. Nikitin, In Situ Synthesis of Al-TiC in Aluminum Melt, *Mater. Lett.*, 2005, **59**, p 2545–2548
3. S.C. Tjong and Z.Y. Ma, Microstructural and Mechanical Characteristics of In Situ Metal Matrix Composites, *Mater. Sci. Eng. R*, 2000, **29**, p 49–113
4. J.F. Shackelford and W. Alexander, *CRC Materials Science and Engineering Handbook*. 3rd ed., CRC Press, Boca Raton, FL, 2001
5. Z.Y. Ma, J.H. Li, S.X. Li, X.G. Ning, Y.X. Lu, and J. Bi, Property-Microstructure Correlation in In Situ Formed Al_2O_3, TiB_2 and Al_3Ti Mixture-Reinforced Aluminum Composites, *J. Mater. Sci.*, 1996, **31**, p 741–747
6. K.L. Tee, L. Lu, and M.O. Lai, In Situ Stir Cast Al-TiB_2 Composite: Processing and Mechanical Properties, *Mater. Sci. Technol.*, 2001, **17**, p 201–206
7. M. Emamy, M. Mahta, and J. Rasizadeh, Formation of TiB_2 Particles During Dissolution of $TiAl_3$ in Al-TiB_2 Metal Matrix Composites Using an In Situ Technique, *Compos. Sci. Technol.*, 2006, **66**, p 1063–1066
8. J. Xu and W. Lu, Wear Characteristic of In Situ Synthesized TiB_2 Particulate-Reinforced Al Matrix Composite Formed by Laser Cladding, *Wear*, 2006, **260**, p 486–492
9. H.W. Huo and S.C. Tjong, Corrosion Behavior of Al-Based Composites Containing In-Situ TiB_2, Al_2O_3 and Al_3Ti Reinforcements in Aerated 3.5% Sodium Chloride Solution, *Adv. Eng. Mater.*, 2007, **9**, p 588–593
10. B.R.W. Hinton, D.R. Arnott, and N.E. Ryan, The Inhibition of Aluminum Alloy Corrosion by Cerous Cations, *Met. Forum*, 1984, **7**, p 211–217
11. D.R. Arnott, B.R.W. Hinton, and N.E. Ryan, Cationic-Film-Forming Inhibitors for the Protection of the AA 7075 Aluminum Alloy Against Corrosion in Aqueous Chloride Solution, *Corrosion*, 1989, **45**, p 12–18
12. A.L. Rudd, C.B. Breslin, and F. Mansfeld, The Corrosion Protection Afforded by Rare Earth Conversion Coatings Applied to Magnesium, *Corros. Sci.*, 2000, **42**, p 275–278
13. A.K. Mishra and R. Balasubramaniam, Corrosion Inhibition of Aluminum Alloy AA 2014 by Rare Earth Chlorides, *Corros. Sci.*, 2007, **49**, p 1027–1044
14. L. Wilson and B.R.W. Hinton, A Method of Forming a Corrosion Resistant Coating, Patent Int WO 88/06639, 1988

15. C. Chen and F. Mansfeld, Corrosion Protection of an Al 6092/SiC_P Metal Matrix Composite, *Corros. Sci.*, 1997, **39**, p 1075–1082
16. A.S. Hamdy, A.M. Beccaria, and P. Traverso, Corrosion Protection of Aluminum Metal Matrix Composites by Cerium Coatings, *Surf. Interface Anal.*, 2002, **34**, p 171–175
17. A. Pardo, M.C. Merino, R. Arrabal, F. Viejo, and M. Carboneras, Influence of Ce Surface Treatments on Corrosion Behaviour of A3xx.x/SiCp Composites in 3.5 wt.% NaCl, *Corros. Sci.*, 2006, **48**, p 3035–3048
18. A. Pardo, M.C. Merino, R. Arrabal, F. Viejo, M. Carboneras, and A.E. Coy, Improvement of Corrosion Behavior of Aluminum Alloy/Silicon Carbide Composites with Lanthanum Surface Treatments, *Corrosion*, 2006, **62**, p 141–151
19. J. Hu, J.X.H. Zhao, S.W. Tang, and M.R. Sun, Corrosion Protection of Aluminum Borate Whisker Reinforced AA 6061 Composite by Cerium Oxide-Based Conversion Coating, *Surf. Coat. Technol.*, 2006, **201**, p 3814–3818
20. S.C. Tjong, G.S. Wang, and Y.W. Mai, Low Cycle Fatigue Behavior of Al-Based Composites Containing In-Situ TiB_2, Al_2O_3 and Al_3Ti Reinforcements, *Mater. Sci. Eng. A*, 2003, **358**, p 99–106
21. S.C. Tjong and G.S. Wang, High-Cycle Fatigue Properties of Al-Based Composites Reinforced with In Situ TiB_2 and Al_2O_3 Particulates, *Mater. Sci. Eng. A*, 2004, **386**, p 48–53
22. S.C. Tjong, G.S. Wang, L. Gen, and Y. W. Mai, Cyclic Deformation Behavior of in situ Aluminum-Matrix Composites of the System Al-Al_3Ti-TiB_2-Al_2O_3, *Compos. Sci. Technol.*, 2004, **64**, p 1971–1980
23. J.Z. Shyu, K. Otto, W.L. Watkins, G.W. Graham, R.K. Belitz, and H.S. Gandhi, Characterization of Pd/γ Alumina Catalyst Containing Ceria, *J. Catal.*, 1988, **114**, p 23–33
24. L.S. Kasten, J.T. Grant, N. Grebasch, N. Voevodin, F.E. Arnold, and M.S. Donley, An XPS Study of Cerium Dopants in Sol-Gel Coatings for Aluminum 2024-T3, *Surf. Coat. Technol.*, 2001, **140**, p 11–15
25. X.W. Yu and G. Li, XPS Study of Cerium Conversion Coating on the Anodized 2024 Aluminum Alloy, *J. Alloy Compd.*, 2004, **364**, p 193–198
26. P. Burroughs, A. Hamnett, A.F. Orchard, and G. Thornton, Satellite Structure in the X-ray Photoelectron Spectra of Some Binary and Mixed Oxides of Lanthanum and Cerium, *J. Chem. Soc. Dalton Trans.*, 1976, **19**, p 1686–1698
27. A. Kotani and A. Ogasawara, Theory of Core-Level Spectroscopy of Rare-Earth Oxides, *J. Electron. Spectrosc. Relat. Phenom.*, 1992, **60**, p 257–299
28. A. Decroly and J.P. Petitjean, Study of the Deposition of Cerium Oxide by Conversion on to Aluminum Alloy, *Surf. Coat. Technol.*, 2005, **194**, p 1–5
29. S.C. Tjong, Self-Passivation of Fe-Cr-PGM Alloys in Reducing Acids Studied by Electrochemical and Electron Spectroscopic Techniques, *Appl. Surf. Sci.*, 1990, **45**, p 301–318
30. M. Bethencourt, F.J. Botana, J.J. Calvino, M. Marcos, and M.A. Rodriguez-Chacon, Lanthanide Compounds as Environmentally-Friendly Corrosion Inhibitors of Aluminum Alloys: A Review, *Corros. Sci.*, 1998, **40**, p 1803–1819